

South Dakota State University

Open PRAIRIE: Open Public Research Access Institutional Repository and Information Exchange

Natural Resource Management Faculty Publications

Department of Natural Resource Management

10-4-2013


Land Surface Phenologies and Seasonalities Using Cool Earthlight in Mid-latitude Croplands

W. G. Alemu

G. M. Henebry

South Dakota State University

Follow this and additional works at: http://openprairie.sdstate.edu/nrm_pubs

 Part of the [Physical and Environmental Geography Commons](#), [Remote Sensing Commons](#), and the [Spatial Science Commons](#)

Recommended Citation

Alemu, W. G. and Henebry, G. M., "Land Surface Phenologies and Seasonalities Using Cool Earthlight in Mid-latitude Croplands" (2013). *Natural Resource Management Faculty Publications*. 16.
http://openprairie.sdstate.edu/nrm_pubs/16

This Article is brought to you for free and open access by the Department of Natural Resource Management at Open PRAIRIE: Open Public Research Access Institutional Repository and Information Exchange. It has been accepted for inclusion in Natural Resource Management Faculty Publications by an authorized administrator of Open PRAIRIE: Open Public Research Access Institutional Repository and Information Exchange. For more information, please contact michael.biondo@sdstate.edu.

Land surface phenologies and seasonalities using cool earthlight in mid-latitude croplands

This content has been downloaded from IOPscience. Please scroll down to see the full text.

2013 Environ. Res. Lett. 8 045002

(<http://iopscience.iop.org/1748-9326/8/4/045002>)

View [the table of contents for this issue](#), or go to the [journal homepage](#) for more

Download details:

IP Address: 137.216.139.53

This content was downloaded on 17/02/2016 at 21:19

Please note that [terms and conditions apply](#).

Land surface phenologies and seasonalities using cool earthlight in mid-latitude croplands

W G Alemu and G M Henebry

Geospatial Sciences Center of Excellence, South Dakota State University, 1021 Medary Avenue, Wecota Hall 506B, Brookings, SD 57007-3510, USA

E-mail: Geoffrey.Henebry@sdstate.edu

Received 29 July 2013

Accepted for publication 18 September 2013

Published 4 October 2013

Online at stacks.iop.org/ERL/8/045002

Abstract

Phenology deals with timing of biotic phenomena and seasonality concerns temporal patterns of abiotic variables. Studies of land surface phenology (LSP) and land surface seasonality (LSS) have long been limited to visible to near infrared (VNIR) wavelengths, despite degradation by atmospheric effects and solar illumination constraints. Enhanced land surface parameters derived from passive microwave data enable improved temporal monitoring of agricultural land surface dynamics compared to the vegetation index data available from VNIR data. LSPs and LSSs in grain growing regions of the Volga River Basin of Russia and the spring wheat belts of the USA and Canada were characterized using AMSR-E enhanced land surface parameters for the period from April through October for 2003 through 2010. Growing degree-days (GDDs) were calculated from AMSR-E air temperature retrievals using both ascending and descending passes with a base of 0 °C and then accumulated (AGDD) with an annual restart each 1 April. Tracking the AMSR-E parameters as a function of AGDD revealed the expected seasonal pattern of thermal limitation in mid-latitude croplands. Vegetation optical depth (VOD), a microwave analog of a vegetation index, was modeled as a function of AGDD with the resulting fitted convex quadratic models yielding both high coefficients of determination ($r^2 > 0.90$) and phenometrics that could characterize cropland differences between the Russian and North American sites. The AMSR-E data were also able to capture the effects of the 2010 heat wave that devastated grain production in European Russia. These results showed the potential of AMSR-E in monitoring and modeling cropland dynamics.

Keywords: microwaves, phenology, remote sensing, AMSR-E, convex quadratic model, European Russia, North America

1. Introduction

Phenology and seasonality are complementary aspects of ecosystem functioning: phenology deals with timing of biotic phenomena; whereas, seasonality concerns temporal patterns

of abiotic variables. Land surface phenology (LSP) describes the timing of vegetated land surface dynamics as observed by remote sensing at spatial resolutions and extents relevant to meteorological processes in the atmospheric boundary layer (de Beurs and Henebry 2004, 2010). In a similar manner, we use the term land surface seasonality (LSS) to describe the timing of abiotic phenomena occurring across the land surface as observed by remote sensing. Examples of LSS include albedo, temperature, soil moisture, soil freeze/thaw, ponding



Content from this work may be used under the terms of the [Creative Commons Attribution 3.0 licence](http://creativecommons.org/licenses/by/3.0/). Any further distribution of this work must maintain attribution to the author(s) and the title of the work, journal citation and DOI.

and flooding, snow cover, and other recurrent and variable aspects of land surface dynamics.

Studies of LSP have long been limited to the visible to near infrared (VNIR) regions, despite degradation by atmospheric effects and solar illumination constraints (Jones *et al* 2012). For example, the normalized difference vegetation index (NDVI; Tucker 1979) is the most commonly used satellite-based vegetation index for studying LSP. It is limited to monitoring the top of the vegetation canopy and the signal is prone to degradation due both to atmospheric effects and to loss of sensitivity over vegetation with high leaf area index (Gitelson 2004, Viña *et al* 2004, Liu *et al* 2011, 2013).

Phenological studies exploiting time series from flux towers have shown the power of the approach, particularly in forested ecosystems (Noormets 2009, Richardson *et al* 2010, Garrity *et al* 2011). Progress has been made recently in linking flux tower data to land surface phenology (Gonsamo *et al* 2012, Kovalskyy *et al* 2012). Both evergreen and deciduous forested ecosystems show consistency in interannual and spatial patterns of sensitivity in annual net ecosystem productivity (NEP) as a function of the carbon uptake period (CUP) characterized by flux tower data (Wu *et al* 2012). However, the CUP was not a good indicator of NEP in non-forested ecosystems, e.g., croplands, grasslands, wetlands (Wu *et al* 2012).

Remote sensing of emitted microwaves, or cool earthlight, provides alternative means for global studies of land surface phenology and seasonality (Jones *et al* 2011, 2012). Microwave radiometers can sense emissions of earthlight at night and through clouds, which leads to increased temporal resolution relative to VNIR imagery, which must be composited to minimize cloud contamination. They can sense both leaf and woody components of aboveground vegetation. Vegetation optical depth (VOD) is a measure of aboveground vegetation canopy thickness using passive microwave remote sensing (Owe *et al* 2001). VOD is less prone to saturation in dense canopies than the NDVI (Liu *et al* 2013). The main disadvantage of passive microwave radiometry is its coarse spatial resolution (25 km in this study) due to low energy emissions (Liu *et al* 2011, 2013, Jones *et al* 2012).

The question we explore here is whether it is possible to apply an LSP model used widely with VNIR data to the advanced microwave scanning radiometer on earth observing system (AMSR-E) products. Geophysical data products derived from passive microwave time series were used to study LSP and LSS in three high-latitude cropland areas: the Volga River Basin in the southeast European Russia, and the spring wheat belts in North Dakota, USA, and in the Prairie Provinces of Canada. We demonstrate that the convex quadratic LSP model well describes the seasonality of air temperature at each site and that the VOD is also well described by the convex quadratic model form. However, the models fits in North America differ substantially from those in Russia.

2. Methodology

2.1. Remote sensing data

The advanced microwave scanning radiometer (AMSR-E) was launched onboard the NASA-EOS Aqua satellite in May 2002. Data from AMSR-E were acquired at both daytime (~1330) and nighttime (~0130) overpasses from mid-June 2002 until its failure in early October 2011. The Numerical Terradynamic Simulation Group (NTSG) at the University of Montana has produced an enhanced land surface parameter suite from AMSR-E data for 2003 through 2010. The data product includes twice-daily air temperatures (t_a ; ~2 m height), fractional coverage of open water over land (fw), vegetation canopy transmittance (tc) at three microwave frequencies, surface soil moisture (mv ; ≤ 2 cm soil depth), and integrated water vapor content of the intervening atmosphere (v) for the total column (Jones and Kimball 2011).

Soil moisture measurement was the primary land surface objective of AMSR-E. Accurate soil moisture retrieval is constrained by vegetation opacity as it reduces the observed microwave sensitivity to soil moisture. The transparency (or transmissivity) of the canopy is inversely related to canopy thickness or vegetation optical depth (VOD) (Owe *et al* 2001). The VOD parameter is a frequency dependent measure of canopy attenuation of microwave emissions due to vegetation biomass structure and water content (Jones *et al* 2012). Lower VOD (higher transmissivity) indicates lower attenuation of soil-emitted microwave radiation by overlying vegetation canopy and vice versa. VOD equal to 0 corresponds to a transmissivity of 1 indicating bare soil, and for dense vegetation the transmissivity gets close to 0 (Owe *et al* 2001, Liu *et al* 2011). A long-term (1988–2008) global vegetation biomass change study on major world biomes found correspondence between VOD and production of major crops (Liu *et al* 2013).

We evaluated eight years (2003–2010) of the air temperature (t_a) and canopy transmittance data in three microwave frequencies: 6.925 GHz (tc_{06}), 10.65 GHz (tc_{10}), and 18.7 GHz (tc_{18}). Over North America, there were many gaps in the VOD retrievals at 6.925 GHz, likely due to radio frequency interference (RFI; Li *et al* 2004, Njoku *et al* 2005). We omitted these data from further analysis and restricted our focus to the two higher frequency VOD retrievals at 10.65 and 18.7 GHz.

2.2. Study areas

To select AMSR-E pixels for analysis, we used the international geosphere biosphere programme (IGBP) global land cover classification scheme in the MODIS land cover product at spatial resolution of 0.05° (MCD12C1). At this coarser resolution each land cover class is available as a percentage cover. In Russia, we selected three AMSR-E pixels near Saratov and one near Volgograd, along the Volga River. For the USA, four pixels were selected in the major spring wheat producing state of North Dakota. In the USA, we also use finer resolution USDA NASS county-level crop

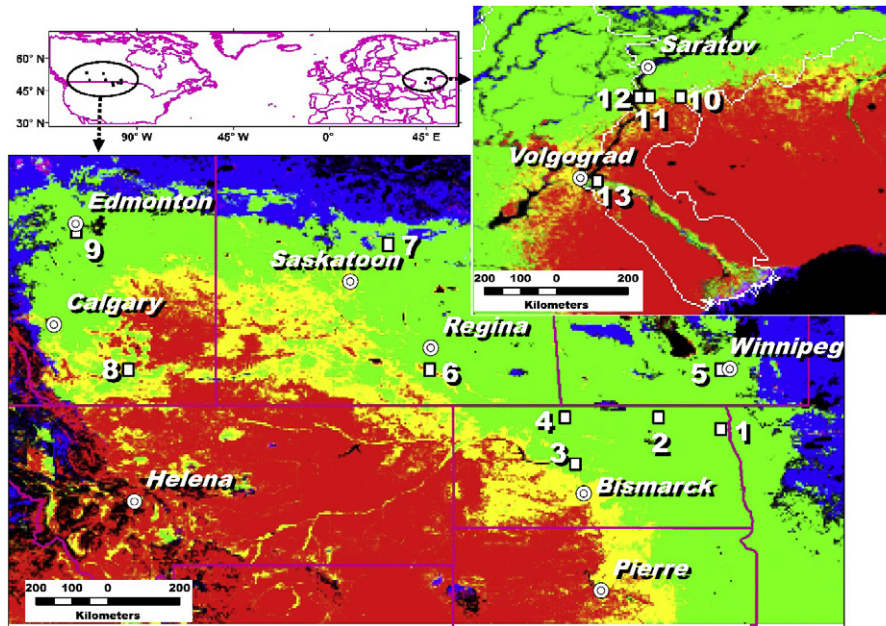


Figure 1. Study area location map (upper left) and land cover map (USA and Canada—bottom, Russia—upper right) superimposed with AMSR-E pixels of the specific study sites: 1 = Grafton, 2 = Munich, 3 = Turtle Lake, 4 = Maxbass, 5 = Winnipeg, 6 = Prince Albert, 7 = Regina, 8 = Lethbridge, 9 = Edmonton, 10 = Saratov 1, 11 = Saratov 2, 12 = Saratov 3, and 13 = Volgograd. Land cover data is from MODIS product MCD12C1 at 0.05° spatial resolution with the maximum of the dominant IGBP land cover class during 2003–2010. Red indicates grasslands; green is croplands, and blue is mixed forest. Yellow indicates a mixture of grasslands and croplands; cyan is a mixture of croplands and mixed forest; and magenta is a mixture of grasslands and mixed forest.

maps (www.nass.usda.gov/Charts_and_Maps/Crops_County/index.asp) to identify spring wheat areas. Five AMSR-E pixels from Canada were selected in the Prairie Provinces of Manitoba, Saskatchewan, and Alberta (figure 1).

2.3. Data processing

The AMSR-E parameters were analyzed from 1st April to 31st October to avoid the frozen season. We applied a 10-day retrospective moving average filter to each parameter time series to minimize data gaps due to orbit and swath width. Meteorological station temperature and rainfall data from NOAA National Climatic Data Center was used for comparative assessment. Additionally, NDVI derived from MODIS MYD09A1 was obtained from the Oak Ridge National Laboratory Distributed Active Archive Center (http://daac.ornl.gov/cgi-bin/MODIS/GR_col5_1/mod_viz.html) for one AMSR-E pixel in one of the Russian cropland sites for comparison with the microwave data.

The thermal regime of growing season can be characterized in terms of accumulated growing degree-days (AGDD; de Beurs and Henebry 2004, 2010, de Beurs *et al* 2009). Growing degree-days were calculated from AMSR-E air temperature data (t_a) using a base temperature of 273.15 K (0 °C) as follows:

$$GDD = \max \left[\frac{t_{a_{day}} + t_{a_{night}}}{2} - 273.15, 0 \right] \quad (1)$$

where $t_{a_{day}}$ and $t_{a_{night}}$ are the air temperatures retrieved during the ascending pass (day) and descending pass (night). The

AGDD were derived from simple summation of the GDD:

$$AGDD_t = AGDD_{t-1} + GDD_t \quad (2)$$

where GDD_t is the daily increment of growing degree-days at day t , and $AGDD_{t-1}$ is the growing degree-days accumulated from the beginning of the study period (here 1 April) until day t .

GDD as a function of AGDD was fitted with a quadratic model:

$$GDD_t = \alpha + \beta AGDD_t + \gamma AGDD_t^2. \quad (3)$$

These three parameters have straightforward interpretations: (1) the intercept α indicates the background GDD value at the beginning of the observation period; (2) the linear parameter β affects the slope; and (3) the quadratic parameter γ controls the curvature. When the fitted model (equation (3)) is convex in shape, i.e., the sign of the β is positive and the sign of the γ is negative, the curve first rises and then falls as thermal time advances.

LSP studies have shown that vegetation index time series, such as the NDVI of herbaceous vegetation in temperate and boreal ecosystems can be readily modeled by a quadratic function of AGDD (de Beurs and Henebry 2004, 2010, Henebry and de Beurs 2013). Here we test if VOD can be modeled in a similar fashion:

$$VOD_t = \alpha + \beta AGDD_t + \gamma AGDD_t^2. \quad (4)$$

The parameter coefficients of the fitted convex quadratic land surface phenology (CxQ LSP) model yield two phenometrics: (1) the peak height (PH), which is the

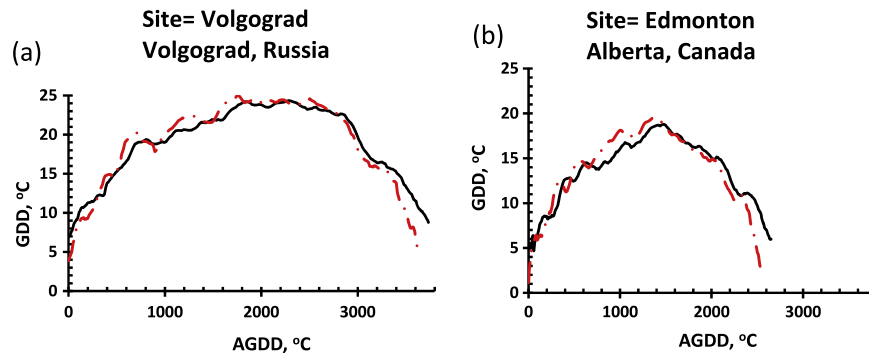


Figure 2. AMSR-E retrieved GDD averaged 2003–2010 (black solid line) as a function of AMSR-E retrieved AGDD averaged 2003–2010 superimposed with similar timespan of meteorological station data (red dash-dotted line) from two study sites. Both AMSR-E time series show a good agreement with the station data; however, the late year divergences may arise from missing AMSR-E retrievals due to frozen surface conditions.

Table 1. Study site name, location, average fitted peak height of growing degree-days (PH_{GDD}), average thermal time to peak GDD (TTP_{GDD}), day of year at peak GDD ($DOY@PH_{GDD}$), and average coefficient of determination for convex quadratic (CxQ) model fits during the period 2003–2010.

Country	Site	Latitude	Longitude	PH_{GDD} (°C)	TTP_{GDD} (°C)	$DOY@PH_{GDD}$	r^2
USA	Turtle Lake	47.54	-101.00	21.5	1772	209	0.96
USA	Grafton	48.41	-97.35	21.1	1707	206	0.98
USA	Maxbass	48.71	-101.26	21.7	1847	211	0.97
USA	Munich	48.71	-98.92	20.4	1616	211	0.98
Canada	Lethbridge	49.90	-112.19	21.1	1803	207	0.92
Canada	Regina	49.90	-104.64	22.6	1836	210	0.96
Canada	Winnipeg	49.90	-97.35	20.4	1608	209	0.97
Canada	Prince Albert	53.04	-105.68	18.2	1416	207	0.98
Canada	Edmonton	53.36	-113.49	17.6	1376	206	0.97
Russia	Volgograd	48.71	44.77	24.0	1943	206	0.97
Russia	Saratov 1	50.82	46.85	26.9	2088	203	0.96
Russia	Saratov 2	50.82	46.07	23.4	1811	204	0.97
Russia	Saratov 3	50.82	45.81	22.9	1781	205	0.97

maximum value in the fitted model or the vertex of the parabola (equation (5)); and (2) the thermal time to peak (TTP), which is the amount of accumulated growing degree-days required to reach the peak height (equation (6)):

$$PH = \alpha - (\beta^2/4\gamma) \tag{5}$$

$$TTP = -\beta/2\gamma. \tag{6}$$

Note that these phenometrics are derived from the parametric model fitted to the data rather than from the data directly.

The VOD time series were modeled in two phases. Convex quadratic models can parsimoniously link GDD as a function of AGDD (figure 2). Thus, in the first phase the TTP_{GDD} was used as a starting point to model VOD, but the duration of the growing period differed between study areas. In the North American sites, peak VODs nearly co-occurred with peak GDDs. Accordingly, we considered the core growing season (CGS) as the period from $0.5 * TTP_{GDD}$ through $1.5 * TTP_{GDD}$, and we fitted the CxQ LSP model using the VOD and AGDD time series from this period. In the Russian sites crops attain their peak VOD very much earlier than peak GDD. Accordingly, we considered core growing season in these croplands to extend from 1st April to date of TTP_{GDD} , and we fitted the CxQ LSP model using the VOD

and AGDD time series from this period. The PH_{VOD} and TTP_{VOD} for all sites were derived using equations (5) and (6), respectively (table 1). Since we want to model VOD based on its own behavior, the TTP_{VOD} derived from the first phase was used to refine the fit of the VOD models. In the second phase, we considered the CGS as the period from $0.5 * TTP_{VOD}$ through $1.25 * TTP_{VOD}$, and we fitted the CxQ LSP model using the VOD and AGDD time series from this period. The PH_{VOD} and TTP_{VOD} metrics reported in table 2 were derived from these second phase models.

3. Results

3.1. Growing degree-days

GDD from AMSR-E and that from weather station data at two study sites compared favorably (figure 2). However, there is some divergence towards the end of the season that likely arises from data gaps due to a lack of AMSR-E retrievals over frozen surfaces.

Behavior of the GDD as a function of AGDD displayed strong seasonality with a convex quadratic shape at each study site (figures 3(a) and 4). Given that mid-latitudes

Table 2. Study site name, coefficient of determination, peak height of VOD, thermal time to peak VOD, and day of year at VOD peak for AMSR-E frequencies 10.65 GHz and 18.7 GHz, respectively, and the difference in growing degree-days between TTP_{VOD} at the two frequencies.

Country	Site	r^2_{VOD10}	PH _{VOD10}	TTP _{VOD10} (°C)	DOY@PH _{VOD10}	r^2_{VOD18}	PH _{VOD18}	TTP _{VOD18} (°C)	DOY@PH _{VOD18}	$\Delta TTP_{VOD18-VOD10}$ (°C)
USA	Turtle Lake	0.99	0.52	1679	205	0.99	0.53	1721	207	42
USA	Grafton	0.99	0.57	2219	228	0.99	0.62	2153	231	66
USA	Maxbass	0.99	0.56	1816	209	0.99	0.57	1843	209	27
USA	Munich	0.99	0.55	1741	217	0.99	0.56	1793	220	51
Canada	Lethbridge	0.98	0.50	1820	223	0.99	0.53	1808	207	-12
Canada	Regina	0.99	0.51	1853	210	0.99	0.54	1843	210	-10
Canada	Winnipeg	0.98	0.53	1735	215	0.99	0.62	2051	231	316
Canada	Prince Albert	0.97	0.60	1686	221	0.98	0.60	1710	223	24
Canada	Edmonton	0.98	0.52	1619	219	0.99	0.55	1629	220	10
Russia	Volgograd	0.97	0.41	1113	168	0.92	0.44	1004	163	-109
Russia	Saratov 1	0.98	0.44	1096	163	0.99	0.47	1067	161	-29
Russia	Saratov 2	0.97	0.42	1032	168	0.94	0.44	991	166	-40
Russia	Saratov 3	0.98	0.43	1142	174	0.98	0.45	1150	175	8

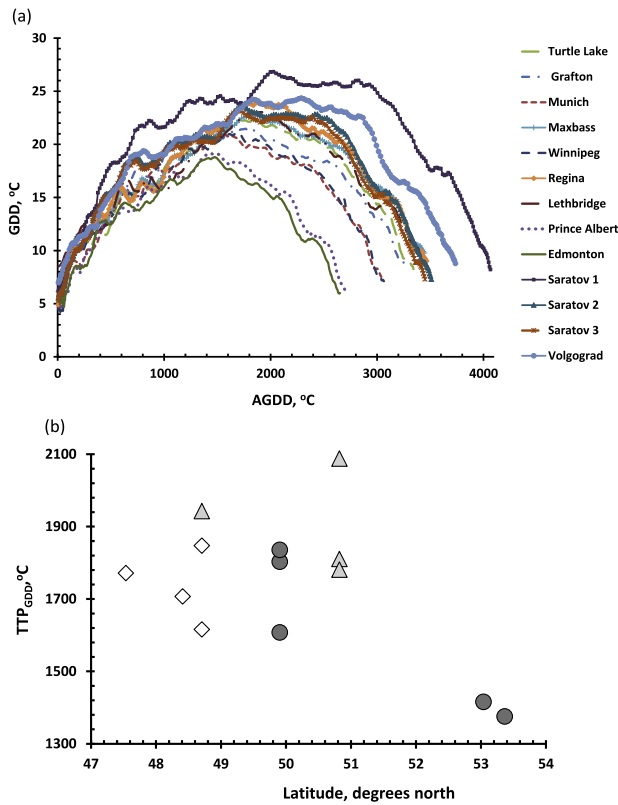


Figure 3. (a) Average AMSR-E GDD (2003–2010) as a function of average AMSR-E AGDD for all study sites. Canadian sites Edmonton and Prince Albert show lower GDD and AGDD due to their northernmost locations. The GDD in the Russian croplands was higher than that in the USA or Canada. (b) Thermal time to peak GDD calculated from parameter coefficients plotted as a function of latitude (hollow diamonds = USA, gray circles = Canada, light gray triangles = Russia). It shows a general decrease in TTP_{GDD} as latitude increases. The uppermost triangle is Saratov 1, which is located relatively far from the Volga River and shows higher TTP_{GDD} , while the three other Russian sites are located along the river.

are temperature limited, this quasi-parabolic relationship during the frost-free period is expected, and the coefficients of determination are uniformly high ($r^2 > 0.90$; table 1,

figure 4). In the USA and Canada croplands, the modeled peak GDD occurred on 27 July (DOY 208) on average; whereas, it occurred four days earlier, on average, in the Volga River basin of Russia (DOY 204) (table 1). While there is an expected inverse relationship between the thermal time at peak GDD (TTP_{GDD}) and latitude, the pattern is relatively weak suggesting that other factors influence the seasonal progression of thermal time (figure 3(b)). The GDDs were higher in Russia than in the North American sites (figures 3 and 4, table 1). The northernmost study sites in Canada, Edmonton and Prince Albert, experienced much lower GDDs. Site Saratov 1 had higher GDD compared to the other three Russia croplands (figure 3(a), table 1); it is located relatively far from the Volga River, while the other three Russian sites are adjacent to the river. Interannual variation in GDD as a function of AGDD appeared higher during the transitional seasons of spring and fall (figure 4).

3.2. Vegetation optical depth

The behaviors of VOD as a function of AGDD exhibit distinct LSPs. During the growing season, VODs ascend to a unimodal peak value and then decline gradually. Peak VOD in the USA and Canada croplands occurred in early August for both frequencies on average. In contrast to the Russian sites the VOD peaks significantly earlier in mid-June (figure 5, table 2). VOD time series showed steep slopes towards their annual peak and then descended gently. The shapes of these seasonal trajectories may reflect microwaves' sensitivity to the timing of vegetation biomass growth and associated changes in canopy water content and the later season drydown and harvest. The pace of fractional green vegetation cover development is quicker than during its disappearance. TTP_{VOD} differences between the AMSR-E two frequencies, 10.65 and 18.7 GHz, was notably higher for Winnipeg (316 AGDD °C) (table 2).

The fitted convex quadratic LSP models for every site for both frequencies showed high coefficients of determination ($r^2 > 0.90$, figure 6, table 2). The Russian sites displayed lower peak VODs that occurred earlier; whereas, the North American sites displayed higher VOD peaks that occurred at

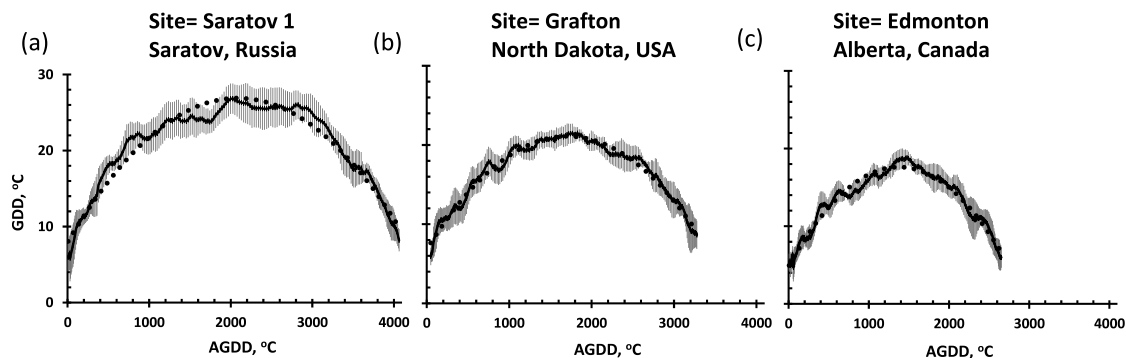


Figure 4. Fitted (dotted lines) average GDD as a function of AGDD superimposed with two standard error GDD error bars (gray crosses) for three croplands for 2003–2010. The coefficients of determination for Saratov 1, Grafton, and Edmonton are 0.96, 0.98, and 0.97, respectively. Interannual variability in GDD tended to be greater in the transitional seasons of spring and fall than in summer. Note the higher interannual uncertainty at the Russian site.

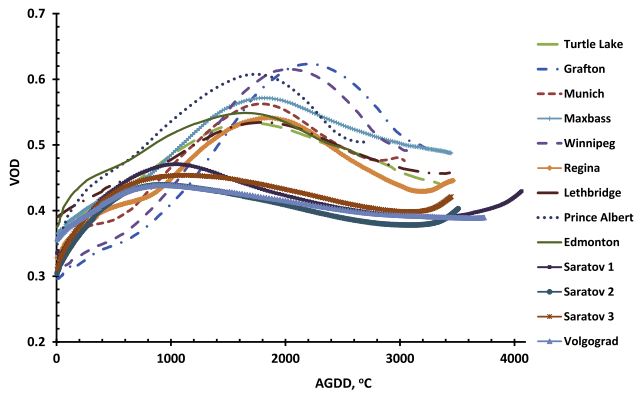


Figure 5. Interannual average (2003–2010) of vegetation optical depth (VOD) as a function of AGDD at the highest AMSR-E frequency. Croplands in Russia attained their peak VOD much earlier than that of the USA and Canada, but with a lower peak and smaller dynamic range.

higher AGDD (figures 5 and 6, table 2). At each study site the VOD peak at the higher frequency (18.7 GHz) was higher than the VOD peak at the lower frequency (10.65 GHz), with the exception of the Prince Albert site, where the peaks were equal in magnitude (table 2). This pattern accords with the fact that the shorter wavelengths are more attenuated by the vegetation canopy and, thus, register higher VOD.

4. Discussion

4.1. VOD and crop type

Peak VOD in Russia occurs much earlier (mid-June) compared to that of the North America (early August) (figure 5, table 2). The North American sites were planted to spring wheat that matures in the first half of August; whereas, the Russian sites were planted to winter grains and some grasses that grow and mature soon after the end of frozen season. Major crops that covered the Volgograd site include winter wheat, while the three Saratov sites were covered by winter wheat and some spring wheat. According to USDA

Foreign Agricultural Service (FAS), each of these Russian sites was within the five major winter wheat producing oblasts that produce more than 60% of the Russian winter wheat crop (USDA FAS 2009). The USDA FAS also indicates that these Russian sites had minimal cover in rye (USDA FAS 2005). The North America croplands had longer growing season and much higher VOD peaks while the Russia croplands exhibited shorter growing season and lower peak VODs. While the difference in peak VOD timing results from phenological differences in winter versus spring grains, the magnitude of the VOD peak suggests differences in cultivation practices and grain varieties as well.

4.2. VOD and land cover

Some cropland sites show distinctive VOD trajectories. For example, the Edmonton site exhibited higher VOD much earlier in the season compared to other Canadian sites. Land cover information, gleaned from MODIS MCD12C1 IGBP 0.05° LC Type 1 percentage, indicates that ~16% of the Edmonton study site falls within suburbs of Edmonton. The earlier season VOD may then result from woods, lawns, parks, and cemeteries in the suburban areas. Other sites having an urbanized component include Winnipeg and Volgograd (~12% each). A study conducted in eastern North America using MODIS NDVI found the effects of urbanized areas on land surface phenology to decay exponentially from the urban boundary to 10 km into rural land covers (Zhang *et al* 2004). Vegetation in urbanized areas can experience longer growing season and lower canopy density compared to those in rural areas, i.e., they have earlier green-up and later dormancy (White *et al* 2002, Zhang *et al* 2004).

4.3. VOD, GDD, and the 2010 Russian heat wave

The effects of the 2010 Russian heat wave (Trenberth and Fasullo 2012) were evident in the AMSR-E time series. At the three Saratov sites, the GDDs were well above the expectation based on the 2003–2009 period, especially at Saratov 1 (figure 7(a)). The VODs were below expectation for much of

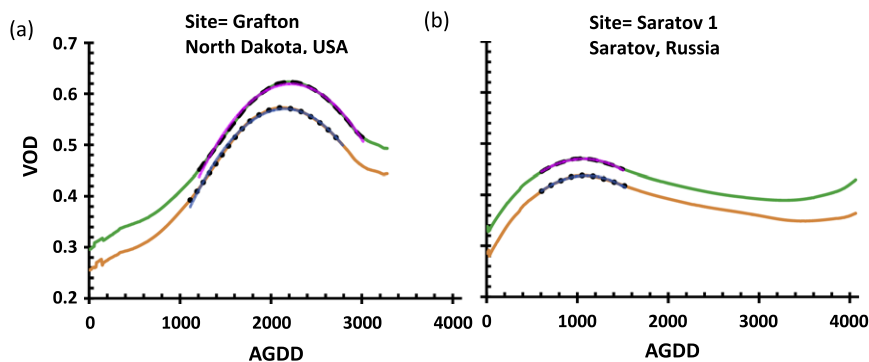


Figure 6. Convex quadratic land surface phenology models for VOD in USA (a) and Russia (b). Green is observed VOD at 18.7 GHz and orange is observed VOD at 10.65 GHz. Black dashed and dotted lines indicate the ‘core growing season’ used to fit each LSP model. The magenta line shows the fitted CxQ model of VOD at 18.7 GHz and the blue line shows the fitted CxQ model of VOD at 10.65 GHz.

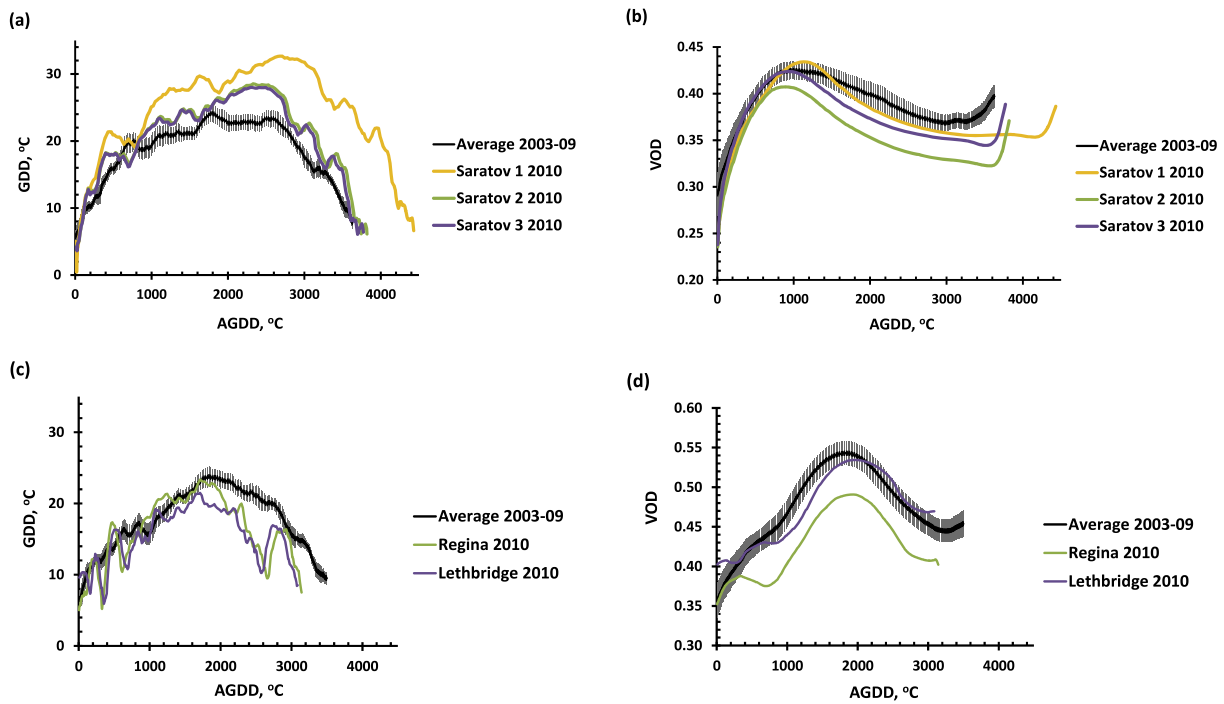


Figure 7. GDD and VOD as a function of AGDD reveal the impact of the 2010 Russian heat wave. The average values are bounded by two standard errors. Saratov 1, 2 and 3 time series show that GDDs were higher in 2010 (a), while the VODs were lower (b). Note the late season upswing in VOD results from fall planting of winter grains. The Regina and Lethbridge sites in Canada, at roughly the same latitude as Saratov, show thermal regimes cooler than expected, especially in the second half of the growing season (c). The VOD trajectory during green-up was significantly below expectation in Lethbridge but recovered during the later season (d). In contrast, at Regina the VOD trajectory was well below expectation (d), despite a similar sequence of GDDs (c). Other factors must account for the depressed VOD trajectory in Regina.

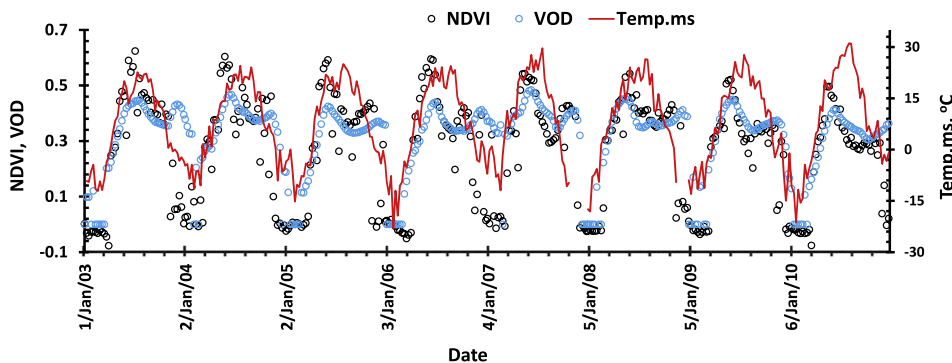


Figure 8. Time series plots of the VOD (cyan circles) and the NDVI (black circles) (2003–2010) from a single AMSR-E pixel, Saratov 1, in Russia. Temperature data (temp.ms) from a nearby meteorological station (red line) is superimposed. The station and VOD data were smoothed with an 8-day retrospective moving average. These data were aligned to the Aqua MODIS MYD09A1 reflectance compositing periods for comparison. All annual data (1 January–31 December) were considered. Notice that the seasonal bimodality of VOD is more pronounced than in the NDVI. The bimodality arises from the planting of winter grains in the fall, and growth and harvest in the subsequent early summer.

the growing season as croplands were negatively impacted by the heat wave (Grumm 2011). Curiously, the VOD trajectory at Saratov 1 was closer to expectation than the other two sites that experienced more modestly elevated temperatures. At two Canadian sites at comparable latitude, the thermal regime was substantially lower than expectation (figure 7(c)). The VODs were significantly depressed at one location (Regina) but not the other (figure 7(d)), despite comparable thermal regimes (figure 7(c)), suggesting that factors other than the temperature affected the Regina LSP. The third Canadian

site at the same latitude, Winnipeg, was not included in the comparison due to the influence of (sub)urban land uses within the AMSR-E pixel.

4.4. VOD compared to NDVI and meteorological station temperature data

Time series analysis of NDVI from Aqua MODIS (calculated from 8-day reflectance) and VOD from AMSR-E (8-day retrospective moving average) for the Saratov 1 site in Russia showed similar LSPs (figure 8). Both indicators of

the vegetated land surface displayed correspondence with temperature data from a nearby meteorological station. The peak in the VOD time series lagged those in the NDVI. This behavior was expected since the VOD is sensitive to canopy water content; whereas, the NDVI is sensitive to photosynthetically active radiation (PAR) absorption (Viña *et al* 2004). Noise in the NDVI time series likely resulted from atmospheric effects, such as sub-pixel cloud contamination. While the NDVI displayed a higher dynamic range than the VOD, the late season secondary peak in winter grains is captured more consistently by the VOD than the NDVI (figure 8). Note how the dynamics in 2010 differ from the earlier years, particularly the long decline in VOD.

An important limitation of the microwave data is its relatively coarse spatial resolution necessitated by the earth's surface low microwave energy emissions, limiting its ability to detect fine spatial scale changes (Liu *et al* 2011, 2013, Jones *et al* 2012). At the same time, the higher temporal resolution of the microwave data offers different insights in the land surface dynamics. Particularly useful is the retrieval of air temperature (rather than skin temperature) at much fine spatial resolution than ground-based meteorological station networks over most of the planetary land surface (although these temperature retrievals are limited in temporal resolution). Although the VOD retrievals span a very large area—nominally 625 km²—the sensitivity to the water content in the vegetated land surface offers a different perspective that may be more temporally responsive to root-zone soil moisture changes than the absorption of PAR which the NDVI indicates. Additional research is needed to investigate how best to use these complementary perspectives for monitoring and modeling the dynamics of the vegetated land surface.

5. Conclusion

Land surface phenologies (LSPs) of VODs and land surface seasonalities (LSSs) of GDDs based on times series of the AMSR-E enhanced land parameters followed seasonal patterns expected from thermally limited croplands. Both the microwave retrieved GDDs and VODs could be well fit using the convex quadratic land surface phenology (CxQ LSP) model that has been successfully applied in many biomes using optical data. The AMSR-E data were also able to detect the impact of the severe heat wave that devastated Russian crops in the summer of 2010. These results show the potential for passive microwave data in general and the AMSR-E enhanced land parameters in particular to be used for modeling cropland dynamics and, possibly, for forecasting agricultural productivity in data sparse regions of the world.

Despite the loss of the AMSR-E, there is a future for information from passive microwave land surface products. The Advanced Microwave Scanning Radiometer 2 (AMSR-2) onboard the Global Change Observations Mission 1st-Water (GCOM-W1), recently renamed SHIZUKU, was successfully launched by Japan Aerospace Exploration Agency (JAXA) in May 2012 and data products were released to the public in May 2013 (<https://gcom-w1.jaxa.jp/>). AMSR-2 has similar functions with AMSR-E, but with some improvements. The

NTSG plans to continue the production of the enhanced land parameters using AMSR-2 datastreams (Kimball 2013). Extending this data record is an important step towards harnessing the power of passive microwave remote sensing for monitoring and modeling landscape dynamics beyond freeze–thaw transitions.

Acknowledgments

This research was supported in part by NASA grants NNX11AB77G and NNX13AN58G. The AMSR-E data were accessed from Numerical Terradynamic Simulation Group (NTSG) website (www.ntsg.umd.edu/project/amsrelp). The MODIS MYD09A1 data were obtained from the Oak Ridge National Laboratory Distributed Active Archive Center (http://daac.ornl.gov/cgi-bin/MODIS/GLBVIZ_1_Glb/modis_subset_order_global_col5.pl). The meteorological data were acquired from NOAA National Climatic Data Center website (<http://gis.ncdc.noaa.gov/map/viewer/#app=cdo&cfg=cdo&theme=temp&layers=1>). We gratefully acknowledge the thoughtful comments from two anonymous reviewers that increased the clarity of the presentation.

References

- de Beurs K M and Henebry G M 2004 Land surface phenology, climatic variation, and institutional change: analyzing agricultural land cover change in Kazakhstan *Remote Sens. Environ.* **89** 497–509
- de Beurs K M and Henebry G M 2010 Spatio-temporal statistical methods for modeling land surface phenology *Phenological Research: Methods for Environmental and Climate Change Analysis* ed I L Hudson and M R Keatley (New York: Springer) chapter 9, pp 177–208
- de Beurs K M, Wright C K and Henebry G M 2009 Dual scale trend analysis distinguishes climatic from anthropogenic effects on the vegetated land surface *Environ. Res. Lett.* **4** 045012
- Garrity S R, Bohrer G, Maurer K D, Mueller K L, Vogel C S and Curtis P S 2011 A comparison of multiple phenology data sources for estimating seasonal transitions in deciduous forest carbon exchange *Agricult. Forest Meteorol.* **151** 1741–52
- Gitelson A A 2004 Wide dynamic range vegetation index for remote quantification of biophysical characteristics of vegetation *J. Plant Physiol.* **161** 165–73
- Gonsamo A, Chen J M, Wu C and Dragoni D 2012 Predicting deciduous forest carbon uptake phenology by upscaling FLUXNET measurements using remote sensing data *Agricult. Forest Meteorol.* **165** 127–35
- Grumm R H 2011 The central European and Russian heat event of July–August 2010 *Bull. Am. Meteorol. Soc.* **92** 1285–96
- Henebry G M and de Beurs K M 2013 Remote sensing of land surface phenology: a prospectus *Phenology: An Integrative Environmental Science* 2nd edn, ed M D Schwartz (New York: Springer) chapter 21, pp 385–411
- Jones L A and Kimball J S 2011 *Daily Global Land Surface Parameters Derived from AMSR-E* (available at <http://nsidc.org/data/nsidc-0451.html>, accessed May 2012)
- Jones M O, Jones L A, Kimball J A and McDonald K C 2011 Satellite passive microwave remote sensing for monitoring global land surface phenology *Remote Sens. Environ.* **115** 1102–14
- Kimball J S 2013 personal communication
- Jones M O, Kimball J S, Jones L A and McDonald K C 2012 Satellite passive microwave detection of North America start of season *Remote Sens. Environ.* **123** 324–33

- Kovalskyy V, Roy D P, Zhang X Y and Ju J 2012 The suitability of multi-temporal web-enabled Landsat data NDVI for phenological monitoring—a comparison with flux tower and MODIS NDVI *Remote Sens. Lett.* **3** 325–34
- Li L, Njoku E G, Im E, Chang P S and Germain K St 2004 A preliminary survey of radio-frequency interference over the US in Aqua AMSR-E data *IEEE Trans. Geosci. Remote Sens. Lett.* **42** 380–90
- Liu Y Y, de Jeu R A M, McCabe M F, Evans J P and van Dijk A I J M 2011 Global long-term passive microwave satellite-based retrievals of vegetation optical depth *Geophys. Res. Lett.* **38** L18402
- Liu Y Y, van Dijk A I J M, McCabe M F, Evans J P and de Jeu R A M 2013 Global vegetation biomass change (1988–2008) and attribution to environmental and human drivers *Glob. Ecol. Biogeogr.* **22** 692–705
- Njoku E G, Ashcroft P, Chan T K and Li L 2005 Global survey and statistics of radio-frequency interference in AMSR-E land observations *IEEE Trans. Geosci. Remote Sens.* **43** 938–47
- Noormets A 2009 *Phenology of Ecosystems Processes* (New York: Springer)
- Owe M, de Jeu R and Walker J 2001 A methodology for surface soil moisture and vegetation optical depth retrieval using the microwave polarization difference index *IEEE Trans. Geosci. Remote* **39** 1643–54
- Richardson A D *et al* 2010 Influence of spring and autumn phenological transitions on forest ecosystem productivity *Phil. Trans. R. Soc. B* **365** 3227–46
- Trenberth K E and Fasullo J 2012 Climate extremes and climate change: the Russian heat wave and other climate extremes of 2010 *J. Geophys. Res.* **117** D17103
- Tucker C J 1979 Red and photographic infrared linear combinations for monitoring vegetation *Remote Sens. Environ.* **8** 127–50
- USDA FAS 2005 *Russia: Agricultural Overview Production Estimates and Crop Assessment Division Report* (available at www.fas.usda.gov/pecad/highlights/2004/11/rs_18nov04/index.htm, accessed July 2013)
- USDA FAS 2009 *Russia: Current Conditions for 2009/10 Winter Grains Commodity Intelligence Report* (available at www.pecad.fas.usda.gov/highlights/2009/03/rs_16march2009/index.htm, accessed July 2013)
- Viña A, Henebry G M and Gitelson A A 2004 Satellite monitoring of vegetation dynamics: sensitivity enhancement by the wide dynamic range vegetation index *Geophys. Res. Lett.* **31** L04503
- White M, Nemani R R, Thornton P E and Running S W 2002 Satellite evidence of phenological differences between urbanized and rural areas of the eastern United States deciduous broadleaf forest *Ecosystems* **5** 260–77
- Wu C *et al* 2012 Interannual and spatial impacts of phenological transitions, growing season length, and spring and autumn temperatures on carbon sequestration: a North America flux data synthesis *Glob. Planet. Change* **92/93** 179–90
- Zhang X, Friedl M A, Schaaf C B, Strahler A H and Schneider A 2004 The footprint of urban climates on vegetation phenology *Geophys. Res. Lett.* **31** L12209